Corey A. Rice, Jan Fulara, Iryna Garkusha, Ádám Nagy,
François-Xavier Hardy, Oliver Gause, and John P. Maier*

Electronic Spectra of Corannulenic Cations and Neutrals in Neon Matrices and Protonated Corannulene in the Gas Phase at 15 K

DOI 10.1515/zpch-2015-0598
Received March 20, 2015; accepted June 14, 2015

Abstract: Three absorption systems starting at 624.1, 601.2, and 590.0 nm were detected in a 6 K neon matrix following deposition of mass selected $m/z = 250$ ions produced from corannulene vapour in a hot cathode ion source. The two latter systems were also observed after deposition of neutral corannulene in solid neon with concomitant bombardment of the matrix with argon ions. The features in the absorption spectrum are assigned to the $4\,^2\mathrm{A}'' \leftarrow X\,^2\mathrm{A}''$ transition of cylobutadieno-benzo[ghi]fluoranthene cation and to the $3\,^2\mathrm{A}' \leftarrow X\,^2\mathrm{A}''$ and $3\,^2\mathrm{A}'' \leftarrow X\,^2\mathrm{A}'$ transitions of two Jahn-Teller structures of bowl-shaped corannulene cations, respectively. The assignment is based on excitation energies calculated with the SAC-CI and CASPT2 methods. The electronic absorption spectrum of protonated corannulene has onsets at 515.1 and 398.8 nm in a neon matrix, following deposition of a mass-selected beam produced by reactions of corannulene with $EtOH_2^+$. The absorptions are assigned, on the basis of theoretical predictions, to the $3{,}4\,^1\mathrm{A} \leftarrow X\,^1\mathrm{A}$ transitions. The electronic spectrum was also recorded in the gas phase using a resonant multiphoton fragmentation technique in an ion trap at vibrational and rotational temperatures of 15 K. The $3{,}4\,^1\mathrm{A} \leftarrow X\,^1\mathrm{A}$ transitions are observed with origin bands at 521 ± 1 nm and 396.4 ± 0.1 nm. The $3\,^1\mathrm{A}$ excited electronic state indicates fast internal conversion of ≈ 5 fs, while the $4\,^1\mathrm{A}$ state has a lifetime of ≈ 0.2 ps. A distinct vibrational pattern is discernible in the $4\,^1\mathrm{A} \leftarrow X\,^1\mathrm{A}$ transition.

***Corresponding author: John P. Maier,** Department of Chemistry, University of Basel, Klingelbergstrasse 80, CH-4056 Basel, Switzerland, e-mail: j.p.maier@unibas.ch
Corey A. Rice, Iryna Garkusha, Ádám Nagy, François-Xavier Hardy, Oliver Gause: Department of Chemistry, University of Basel, Klingelbergstrasse 80, CH-4056 Basel, Switzerland
Jan Fulara: Institute of Physics Polish Academy of Sciences, Al. Lotników, 32/46, PL-02-668, Warsaw, Poland

Keywords: Electronic Spectroscopy, Matrix Absorption Spectroscopy, Corannulene Cation, Protonated Corannulene, Ion Traps.

Dedicated to Prof. Dr. Dr. h.c. mult. Jürgen Troe on the occasion of his 75th birthday

1 Introduction

Polycyclic aromatic hydrocarbons (PAHs) are important in terrestrial environments as they are produced in combustion processes and lead to soot formation [1]. They are also of astrophysical interest, appearing to play a major role in the interstellar medium (ISM), because of their association with the unidentified infrared (UIR) bands [2]. Presently, more than 150 molecules have been confirmed to be in the ISM [3, 4], mainly by the analysis of pure rotational transistions. However, some species cannot be observed by radio astronomy because of the lack of a permanent electric dipole moment. Astronomical spectra in the IR and visible may be a technique to prove there existence in the ISM. However, no individual molecule is the cause of these IR features. PAH cations and their derivatives have also been proposed as candidates for the diffuse interstellar bands [5, 6], though to date, no specific PAH has been identified.

Corannulene, $C_{20}H_{10}$, is the smallest known PAH adopting a bowl-like structure composed of five pericondensed benzene rings around a central cyclopentadienyl unit. It is a highly symmetric molecule, C_{5v}, with a dipole moment of 2.1 D [7]. It has been studied by microwave spectroscopy and its rotational transitions were sought using radio astronomy, but without success [8]. $C_{20}H_{10}$ resembles a fragment of C_{60} and could be an intermediate in its formation, given that fullerenes were detected in planetary nebulae [9, 10].

Recently, there is a growing interest among organic chemists in functionalizing corannulene [11–14]. Several reactive corannulene carbocations $C_{20}H_{10}$-R^+ (R = -methyl, -chloromethylene, -dichloromethine, -CCl_3 and -CH_2CH_2Cl, Br) were synthesised in a reaction of corannulene with halogenated hydrocarbons in the presence of Lewis acids [12, 15]. $C_{20}H_{10}$-R^+ were isolated as salts with anions in solutions and solids and were characterized by the H/^{13}C NMR and UV-Vis spectroscopy, as well as X-ray diffraction [12, 15]. These and theoretical studies [16] revealed that R^+ binds to the inner five-membered ring of corannulene (*hub*-position), while -CCl_3^+ prefers the peripheral benzene carbons (rim). The [$C_{20}H_{10}$-R^+, $AlCl_4^-$] salts in organic solvents exhibits strong, broad absorptions in the visible range, e.g. $C_{20}H_{10}$-CH_3^+ at 560 nm in $CDCl_3$ [15]. Though electronic spectra of complex $C_{20}H_{10}$-R^+ carbocations have been reported in solution, there

are no data on the simplest systems: $C_{20}H_{10}^{+}$ and $C_{20}H_{11}^{+}$. These cations have only been measured in the IR using a free electron laser and compared with planar PAHs [17].

Herein, the electronic absorption spectra of protonated corannulene and its neutral radical counterpart, following mass selection and deposition in 6 K neon matrices are presented. The electronic spectrum of protonated corannulene could also be recorded in the gas phase at 15 K using an ion trap.

2 Methods

2.1 Experimental

Corannulene, $C_{20}H_{10}$, was synthesised via a solution-phase reaction [18]. Two experimental techniques were employed to obtain the electronic spectra of corannulene species. A gas-phase method which uses the confinement capabilities of an ion trap was used for protonated corannulene. The other in the condensed phase utilises a mass selector to embed cations in a 6 K neon matrix.

2.2 6 K neon matrix

The setup employed for mass-selected matrix isolation of ions is described elsewhere [19]. Cations were produced in a hot cathode discharge source from $C_{20}H_{10}$ mixed with helium. Ions were extracted and guided through an electrostatic bender to a quadrupole mass selector (QMS). The $m/z = 250$ ions passed through the QMS and were codeposited with a mixture of neon and CH_3Cl (in a 20 000 : 1 ratio) onto a rhodium-coated sapphire plate held at 6 K. CH_3Cl acts as an electron scavenger, compensating the positive charge. After a ≈ 150 μm thick matrix was produced, electronic absorption spectra were measured in the 250–1000 nm range by passing broadband radiation through crystalline neon, parallel to the matrix substrate. The light was wavelength-dispersed by a 0.3 m spectrograph and detected with a CCD camera. A photobleaching procedure was employed to distinguish absorptions of cations from those of neutrals. The neon matrix was irradiated with UV light from a medium pressure mercury lamp. Electrons from Cl^{-}, produced from CH_3Cl, are set free and neutralise positive species. Absorptions which decrease upon UV irradiation have a cationic origin, whereas those which gain in intensity are due to uncharged molecules.

Corannulene cation was also generated by Ar^+ bombardment of a neon matrix containing $C_{20}H_{10}$. A charge-exchange reaction yields $C_{20}H_{10}{}^+$, thus the desired cation is produced by a gentler ionization than in the source. The excess energy of this reaction is dispersed into vibrational degrees of freedom and then to the 6 K neon environment.

The protonation reaction $C_{20}H_{10} + C_2H_5OH_2{}^+ \rightarrow C_{20}H_{11}{}^+ + C_2H_5OH$ was used to produce $C_{20}H_{11}{}^+$ in the same source. The exothermicity of the H^+ transfer is due to the difference in proton affinities of ≈ -70 kJ, mol^{-1} [20].

2.3 22-pole ion trap

Protonated corannulene, $C_{20}H_{11}{}^+$, was generated by heating solid corannulene to ≈ 340 K, followed by bombardment with 35–40 eV electrons in a toluene atmosphere within a chemical ionization (CI) source. The proton affinity of C_7H_8 is lower than that of $C_{20}H_{10}$, leading to the exothermic reaction $C_7H_9{}^+ + C_{20}H_{10} \rightarrow C_{20}H_{11}{}^+ + C_7H_8$. Other protonated species, such as $C_7H_9{}^+$, were also created through ion-molecule reactions.

The apparatus employed has been described [21]. Ions from a CI source were deflected by 90° and injected into a 440 mm long radio frequency (rf)-only 6-pole in order to narrow the kinetic energy distribution of the cations from the CI source by collisions with helium. $C_{20}H_{11}{}^+$, $m/z = 251$, was mass-selected by a quadrupole (± 0.5 u) and electrostatically turned by 90° into an rf-only octupole and then transported into a 22-pole rf trap [22], thermalizing cations for ≈ 50 ms with 6 K helium buffer gas (one collision per microsecond). This was followed by laser irradiation, extraction and analysis by a second quadrupole.

The dissociation yield of $C_{20}H_{10}{}^+$ was monitored as a function of laser wavelength to obtain the electronic spectrum of $C_{20}H_{11}{}^+$. Radiation from a tunable dye laser (0.07 cm^{-1} bandwidth with ≈ 5 mJ energy per pulse) was used to record the rotational contour of the origin band and excited state vibrational transitions. The spectrum was calibrated with an external wavemeter and power corrected.

2.4 Computational

Equilibrium coordinates of the lowest energy $C_{20}H_{10}{}^+$ and $C_{20}H_{11}{}^+$ isomers (Chart 1SI and 2SI) and their neutrals were calculated with density functional theory (DFT) using the PBE0 functional [23, 24] and cc-pVDZ basis set [25]. For selected isomers the B3LYP functional [26, 27] was also applied to compare the results with the literature data obtained with a larger basis set [28]. The calcu-

lations have been carried out with the Gaussian 09 program package [29]. Vertical excitation energies of species with a singlet ground state were calculated with time dependent (TDDFT), symmetry-adapted cluster configuration interaction (SAC-CI) [30, 31] implemented in Gaussiann 09, and multistate multiconfigurational second-order perturbation (MS-CASPT2) methods [32], the latter uses the Molcas software [33]. For molecules with a doublet multiplicity ground state the two latter methods were used. To obtain dipole-allowed electronic transitions with energy below 5 eV, a different number of calculated roots were chosen – the higher the molecular symmetry the smaller number of excited states was calculated. SAC-CI calculations were computed with unrestricted Hartree–Fock (UHF) for singlets and restricted open-shell HF (ROHF) for doublets. About 300 orbitals with an energy < 3 Hartree were exploited. In CASPT2 calculations, state averaging was utilised; wavefunctions were optimized for the mean energy of the electronic states computed (usually 5–8 states depending on symmetry of molecule). An active space was constructed from twelve electrons distributed over twelve orbitals (12,12) in case of singlets and (11,12) for doublets.

3 Results and discussion

3.1 Corannulene cation and neutral

Mass selected deposition of $C_{20}H_{10}^{+}$ ions ($m/z = 250$) in a neon matrix produces the spectrum shown in Figure 1 (blue trace). Strong absorptions are present in the 540–630 nm and 290–410 nm regions. The features in the visible diminish, whereas the ones in the UV increase upon irradiation of the matrix with $\lambda > 260$ nm photons (red trace). This suggests that the former originate from the cationic carrier and the latter belong to a neutral molecule. The prominent band at 624.1 nm and the absorption system starting at 601.2 nm decay at a different rate upon UV irradiation; hence, they belong to two cationic species. Scaling the spectra measured after deposition of $m/z = 250$ cations and after irradiation to the intensity of the 624.1 nm band and subtracting each other, a 'clean' absorption system with an onset at 601.2 nm is obtained (magenta trace of Figure 2). Repeating the same procedure when the 601.2 nm band is normalized, the 'clean' 624.1 nm absorption system is produced (green trace, Figure 2). The wavelengths of the band maxima of the two cationic species are collected in Table 1.

In another experiment, corannulene (Cora) vapour was trapped in solid neon with concomitant bombardment of the neon surface with a 20 nA beam of Ar^{+}. The spectrum obtained is shown in the black trace of Figure 2 and is identical with

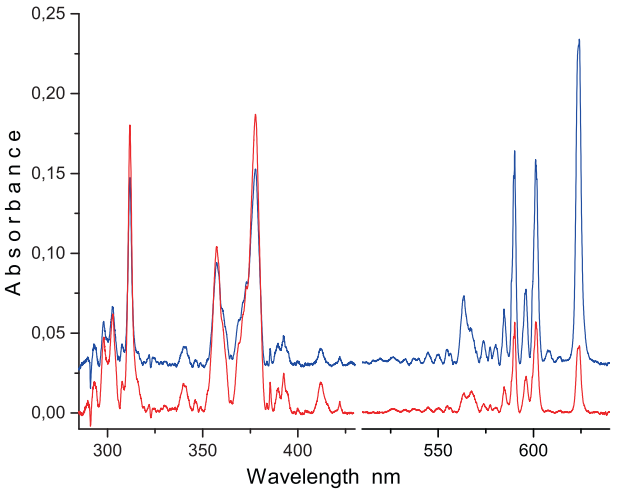

Figure 1: Electronic absorption spectra recorded after deposition of mass selected $C_{20}H_{10}^{+}$ ions produced from corannulene vapour in a hot cathode ion source and trapped in a 6 K neon matrix (blue trace) and after subsequent irradiation with $\lambda > 260$ nm photons (red trace). Absorptions which diminish after UV irradiation originate from cations and those which gain in intensity are due to neutral species.

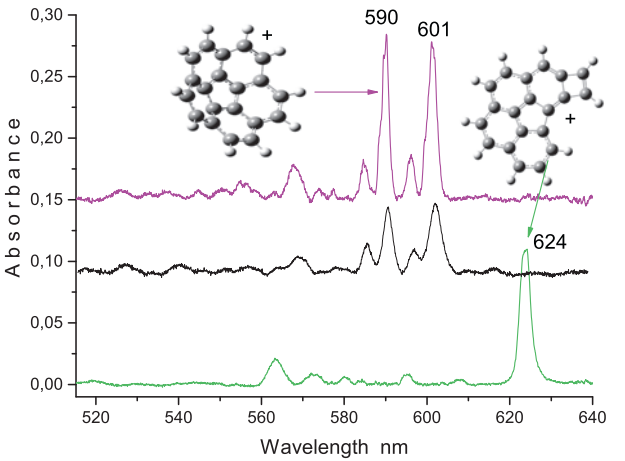

Figure 2: Absorption spectrum of corannulene cation in a 6 K neon matrix (magenta trace) obtained after scaling the spectra shown in Figure 1 to the intensity of the 624 nm band and subtracting the blue trace from the red one. The green trace shows the $4\,^2A'' \leftarrow X\,^2A''$ electronic transition of planar $C_{20}H_{10}^{+}$ cation obtained using the same procedure by normalizing to the 601.2 nm band. The black trace was obtained after deposition of neutral corannulene in a neon matrix and ionization with argon ion beam.

Table 1: Band maxima (± 0.1 nm) in the electronic absorption spectrum of corannulene cation and isomer $CBBF^+$ observed in a 6 K neon matrix and suggested assignment.

λ/nm	λ^{-1}/cm^{-1}	$\Delta\tilde{\nu}$/cm^{-1}	Assignment
Isomer $CBBF^+$			
624.1	16 023	0	$4\,^2A'' \leftarrow X\,^2A''$
613.5	16 300	277	
608.2	16 442	419	
595.1	16 804	781	
580.1	17 238	1215	
572.6	17 464	1441	
563.5	17 746	1723	
$Cora^+$			
601.2	16 633	0	$3\,^2A' \leftarrow X\,^2A''$
596.1	16 776	143	
590.0	16 949	0*	$3\,^2A'' \leftarrow X\,^2A'$
584.6	17 106	157*	
577.3	17 322	689	
573.8	17 428	795	
567.7	17 615	982	
556.5	17 969	1020*	
554.6	18 031	1398	
549.9	18 185	1552	
544.5	18 365	1732	

* bands belong to the 590 nm system of $Cora^+$

the 601.2 nm absorption system. The strong band at 624.1 nm and the weaker ones that belong to this system are absent in the spectrum. The experiment proves that two cationic species are present in the matrix after trapping mass selected $C_{20}H_{10}{}^+$. The 601.2 nm absorption system corresponds to the electronic transition of $Cora^+$ because the cations are formed under milder conditions than in the ion source, i.e. via a charge-exchange reaction of Cora with Ar^+, where the excess energy is dissipated to a neon lattice. The absorption system starting at 624.1 nm likely belongs to a higher energy isomer of $C_{20}H_{10}{}^+$, formed in the ion source or during trapping into solid neon.

Neutral coranulene (Cora) was deposited in a neon matrix and the spectrum obtained is the magenta trace of Figure 3. Absorptions were detected in the 340–420 nm range. Below 340 nm the matrix was not transparent due to light scattering or strongly absorbing species. Cora was studied previously in an argon matrix. An intense feature is seen at 249.5 nm and two weaker systems around 284.5 and 337.5 nm were observed [28]. The absorptions were assigned to opti-

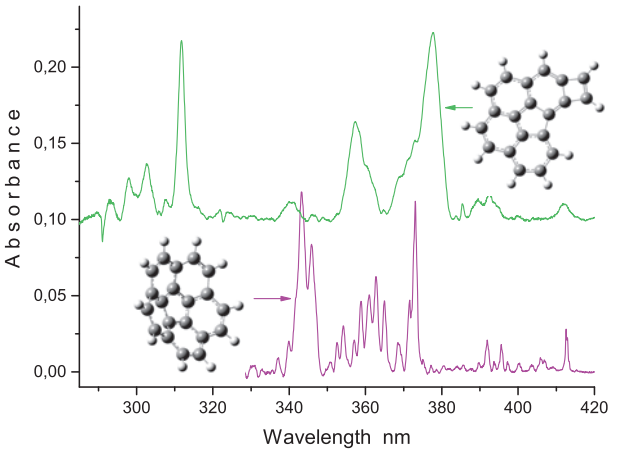

Figure 3: Electronic absorption spectrum of neutral corannulene (magenta trace) measured after deposition of the neutral corannulene in a 6 K neon matrix. Green trace shows the absorption spectrum of planar $C_{20}H_{10}$ obtained after deposition of mass selected $C_{20}H_{10}^{+}$ and subsequent UV irradiation.

cal transitions of the $2\,^1E_1$, $1\,^1E_1$ and $1\,^1A_1$ excited states from the $X\,^1A_1$ ground state of Cora, based on TD DFT calculations. There are also three lower energy electronic states, $1\,^1A_2$, $1\,^1E_2$ and $2\,^1E_2$ at 3.53, 3.56, and 3.83 eV, which are not dipole accessible from the ground state. Absorptions detected in the present study are in the range where forbidden transitions are expected. The detection system used here is about two orders of magnitude more sensitive than that in the previous study [28] due to a longer path length, ≈ 20 mm, compared to a fraction of a mm in traditional matrix isolation. The high sensitivity enables the detection of weak transitions. Moreover, symmetry forbidden transitions in the gas phase can become allowed in the matrix due to perturbations by the neon environment.

Vertical excitation energies of Cora were calculated with the TDDFT, SAC-CI and MS(8)-CASPT2 (12,12) methods. TDDFT give the same results [28] though a larger basis set (cc-pVTZ) was used in the latter. The excitation energies calculated with three methods are presented in Table 2. TDDFT and SAC-CI give a similar order of excited states except that the $1\,^1A_2$ and $1\,^1E_2$ states are reversed. CASPT2 calculations have been carried out in C_s symmetry, and as a result the formerly forbidden transitions become allowed with low oscillator strengths. The vertical excitation energies calculated with the three methods agree with the neon matrix transitions of Cora.

After irradiating the matrix with $\lambda > 260$ nm photons, the absorption spectrum of neutral species produced from electron recombination is obtained (Fig-

Table 2: Vertical excitation energies in eV and oscillator strengths of the electronic transitions of neutral isomers of $C_{20}H_{10}$. Cora and CBBF calculated with the TDDFT, SAC-CI, and CASPT2 using the equilibrium coordinates obtained from DFT/PBE0.

	Cora			CBBF		
State	TDDFT	SAC-CI	CASPT2	TDDFT	SAC-CI	CASPT2
$1\,^1A'$	3.62 0.0	3.72 0.0	3.92 0.001	2.66 0.004	2.53 0.01	3.19 0.03
$2\,^1A'$	3.66 0.0	3.72 0.0	3.93 0.001	3.15 0.04	3.04 0.05	3.66 0.06
$3\,^1A'$	3.66 0.0	3.81 0.0	4.17 0.02	3.35 0.001	3.60 0.006	3.96 0.02
$4\,^1A'$	3.93 0.0	4.15 0.0	4.35 0.04	3.69 0.007	3.84 0.03	4.31 0.03
$5\,^1A'$	3.93 0.0	4.16 0.0	4.45 0.1	3.88 0.05	4.17 0.2	4.75 0.04
$6\,^1A'$	4.16 0.01	4.47 0.03	4.68 0.04	4.04 0.03	4.37 0.09	4.79 0.002
$7\,^1A'$	4.48 0.3	4.74 0.3	4.80 0.3	4.19 0.06	4.66 0.2	5.30 0.04
$8\,^1A'$	4.48 0.3	4.76 0.3	5.05 0.1	4.28 0.1	4.78 0.1	
$9\,^1A'$	5.42 0.3	5.68 1	5.90 0.3	4.62 0.7	4.93 0.9	
$10\,^1A'$	5.42 0.3	5.70 1	6.11 0.3	4.75 0.1	5.42 0.4	

ure 3, green trace). The neon lattice efficiently quenches the excitation energy during neutralization of cations; therefore, the structure of the molecular ion is retained upon charge cancellation. The bands of Cora are barely observable, suggesting that the oscillator strengths of the 601.2 and 590.0 nm systems of $Cora^+$ are stronger than the one of the forbidden transition of Cora in the 340–420 nm range. The new absorptions detected in the same spectral region as that of Cora (magenta trace) belong to the neutral counterpart of the other cation responsible for the 624 nm system.

Two absorption bands at 601.2 and 590.0 nm dominate the spectrum of $Cora^+$. The 590.0 nm band lies 316 cm^{-1} above onset of the system. $Cora^+$ possesses several low frequency vibrations. DFT calculations, using B3LYP functional and cc-pVDZ basis set, predict two normal modes of energy 295 and 305 cm^{-1} (Table 1SI) close to the value 316 cm^{-1} derived from the spectrum. However, the relative intensities of these two bands in the spectrum of $Cora^+$ suggest that the overtone of 316 cm^{-1} around 579 nm should also be detected in contrast to the observation. Therefore, the 601.2 and 590.0 nm absorptions belong to two different electronic systems. Two weaker bands $\approx$ 150 cm^{-1} above each origin are present in the spectrum shown in magenta in Figure 2. This energy is close to the 143 cm^{-1} ground state frequency of $Cora^+$ calculated with the DFT method. The other pair of bands $\approx$ 1000 cm^{-1} above the origins is also observed in Figure 2.

To deduce whether these two systems are two electronic transitions of $Cora^+$, or belong to two structures of the cation, calculations of the excitation energies have been carried out with the SAC-CI and MS(8)-CASPT2 (11,12) methods using the DFT/PBE0 coordinates. Vertical excitation energies of $Cora^+$ obtained in

Table 3: Vertical excitation energies in eV and oscillator strengths of the electronic transitions of Cora$^+$ and CBBF$^+$ calculated with SAC-CI and MS(8)-CASPT2 (11,12) using geometries from DFT/PBE0.

	Cora$^+$ $X\,^2A''$		CBBF$^+$ $X\,^2A''$	
State	SAC-CI	CASPT2	SAC-CI	CASPT2
$1\,^2A''$	0.44 0.001	0.46 0.01	1.04 0.003	1.09 0.03
$2\,^2A''$	2.84 0.001	2.68 0.002	1.47 0.007	1.63 0.004
$3\,^2A''$	3.51 0.002	3.53 0.007	1.82 0.03	1.90 0.05
$4\,^2A''$	3.68 0.004	3.94 0.1	2.87 0.09	1.97 0.05
$5\,^2A''$	4.74 0.005	4.15 0.02	3.80 0.01	2.76 0.06
$6\,^2A''$	5.66 0.0	4.35 0.001	4.51 0.001	3.25 0.04
$7\,^2A''$		5.45 0.06	3.33 0.06	
$1\,^2A'$	0.36 0.001	0.34 0.02		
$2\,^2A'$	0.48 0.0	0.95 0.004		
$3\,^2A'$	2.78 0.2	2.24 0.2		
$4\,^2A'$	3.03 0.007	2.59 0.02		
$5\,^2A'$	3.51 0.001	3.55 0.06		
$6\,^2A'$	3.94 0.0	3.62 0.04		
$7\,^2A'$	5.03 0.0	4.21 0.05		

these calculations are compared in Table 3. Both calculations predict a strong $3\,^2A' \leftarrow X\,^2A''$ electronic transition of Cora$^+$ in the visible region: CASPT2 at 2.24 eV and SAC-CI at 2.78 eV, which can be compared with the experimental value 2.06 eV. There is no other intense transition around this energy. The other intense $4\,^2A'' \leftarrow X\,^2A''$ transition is predicted at 3.94 eV by CASPT2, which was not detected in this experiment, and the large oscillator strength, $f = 0.12$, can be an artefact of the method. The CASPT2 diagnostic tools indicate that the active space used (11,12), is too small to accurately describe higher excited states of Cora$^+$ due to a number of low energy occupied orbitals in the cation. In the case of SAC-CI calculations, ≈ 300 orbitals were used and the results obtained are more reliable, though the excitation energies are overestimated by ≈ 0.7 eV.

Because only one strong transition is predicted in the visible range, the 601.2 and 590 nm systems are due to different structures of Cora$^+$. Neutral corannulene has C_{5v} symmetry and an e_2 HOMO. Upon ionization, the degeneracy of the e_2 orbitals is removed by a Jahn–Teller (JT) distortion in the $X\,^2E_2$ ground state. The C_{5v} geometric structure is compressed or elongated with respect to the σ_v mirror plane, resulting in an electronic ground state of either $^2A'$ or $^2A''$ symmetry. $C_{20}H_{10}{}^+$ has five C_s minima located around the C_{5v} JT conical intersection. The barrier between the minima has been estimated to be 18 cm^{-1} in $C_{20}H_{10}{}^-$, via ESR spectroscopy [35]. The computed energy barrier for $C_{20}H_{10}{}^+$ using a DFT method

is 6 cm^{-1} [17]. Therefore, the pseudo-rotation in $C_{20}H_{10}^{-}$ would be expected in $C_{20}H_{10}^{+}$ as well, resulting in a dynamic JT effect. Because the barrier is low, two forms (A′ and A″) of $Cora^{+}$ are trapped in the matrix and the 601.2 and 590 nm absorption systems are assigned to the $3\,^2A' \leftarrow X\,^2A''$ and $3\,^2A'' \leftarrow X\,^2A'$ electronic transitions of these JT distorted structures.

The carrier of the prominent 624 nm absorption system is an isomer of $C_{20}H_{10}^{+}$ which is produced in the ion source, or during deposition, at energies of ≈ 50 eV. If a fragment is responsible for the 624 nm band, the most plausible candidate is $C_{20}H_9^{+}$, formed by a cleavage of the C–H bond. Vertical excitation energies of $C_{20}H_9^{+}$ were calculated with TDDFT, SAC-CI, and MS(8)-CASPT2 and for neutral $C_{20}H_9$ using the latter two methods. The results are shown in Table 2SI. $C_{20}H_9^{+}$ and $C_{20}H_9$ possess weak electronic transitions which do not match neither the 624 nm nor the UV systems.

A candidate for the 624 nm absorption is another isomer of $C_{20}H_{10}^{+}$. One is A^{+}, benzo[ghi]fluoranthene cation with an ethynyl group attached, and can be formed by cleavage of one benzene ring of $Cora^{+}$. The realitive energy is predicted 125 kJ, mol^{-1} above $Cora^{+}$ at the DFT/PBE0 level. The excitation energies of A^{+} and A calculated in similar manner, as in the case of $C_{20}H_9^{0/+}$, are shown in Table 3SI. They do not correlate with the observations.

Three other isomers ($B^{+} - D^{+}$) of $C_{20}H_{10}^{+}$ were also considered as carriers of the 624 nm system (Chart 1SI). B^{+}, C^{+}, and D^{+}, fluoranthene cations with two ethynyl groups, can be produced from $Cora^{+}$ by cleavage of two benzene rings. They lie ≈ 300 kJ, mol^{-1} above $Cora^{+}$. Excitation energies of these isomers were calculated with SAC-CI and CASPT2 and results are given in Tables 4SI. The strongest, lowest energy transitions of these cations are predicted in the near infrared at 1.2–1.5 eV – far from the observation (1.99 eV); therefore, the 624 nm system does not originate from these cations.

Isomer $CBBF^{+}$ (Chart 1SI) is 91 kJ, mol^{-1} above $Cora^{+}$ in energy, having a similar structure to A^{+}. The geometry of A^{+} has an ethynyl group, forming a four member carbon ring with an adjacent benzene ring and migration of one hydrogen atom. SAC-CI calculations predict a moderately intense ($f = 0.089$) electronic transition for this cation 2.86 eV close to the predicted 2.87 eV for $Cora^{+}$ with this method (Table 3). MS(8)-CASPT2 (11,12) calculations predict three moderately intense transitions in the 1.90–2.76 eV energy range close to the observation at 1.99 eV (624 nm). However, due to a small active space limited by computational reasons, and a number of low energy occupied orbitals of $CBBF^{+}$, the CASPT2 results give a crude approximation of the energy levels of the cation. Vertical excitation energies of neutral CBBF using the TDDFT, SAC-CI, and MS(8)-CASPT2 (Table 2) revealed that this is the only structure which can be responsible for the absorptions detected in the 310–400 nm range after deposition of mass-

selected $C_{20}H_{10}^{+}$ in a neon matrix (Figure 3). The most prominent absorptions are observed at around 313, 358, and 378 nm – 3.96, 3.46, and 3.28 eV, respectively, which are close to moderately intense electronic transitions of CBBF at 4.17, 3.84, and 3.04 eV predicted by SAC-CI and at 3.96, 3.64 and 3.19 eV according to CASPT2. Therefore, the 624 nm band system is assigned to the $4\,^2A'' \leftarrow X\,^2A''$ electronic transition of $CBBF^+$ and the UV absorptions at 313, 358, and 378 nm to the $4,3,2\,^1A' \leftarrow X\,^1A'$, respectively.

3.2 Protonated corannulene

3.2.1 6 K neon matrix

Deposition of $m/z = 251$ cations produced in the reaction of Cora with $EtOH_2^{+}$ resulted in strong absorptions starting at 398.8 nm and an order of magnitude weaker system at 707.0 nm (Figure 4, blue trace). The 399 nm system diminishes while the one at 707 nm gains in intensity after irradiation $\lambda > 260$ nm of the matrix (red trace), pointing to a cationic carrier of the former and neutral for the latter. Weak absorptions of $Cora^+$ at 624.1, 601.2, and 590.0 nm overlap with

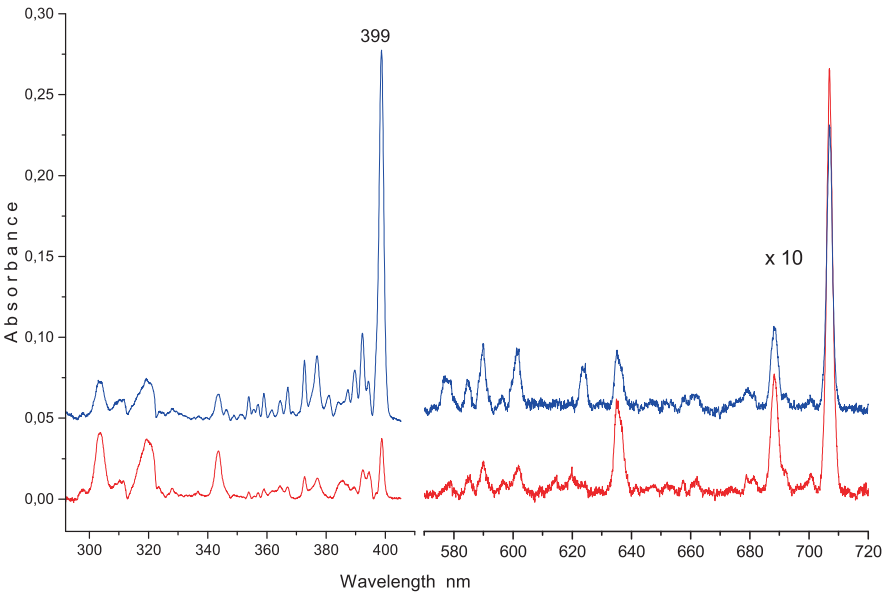

Figure 4: Electronic absorption spectra recorded after deposition of mass selected $C_{20}H_{11}^{+}$ in a 6 K neon matrix (blue trace) and after neutralization of ions with $\lambda > 260$ nm photons (red trace).

the 707 nm system. These are present either because the ^{13}C isotopologue has the same mass as protonated corannulene ($HCora^+$), or are due to an insufficient mass resolution. The 399 and 707 nm systems are unique for deposition of $m/z = 251$ ions. A number of protonated PAHs (of naphthalene [36], anthracene, phenanthrene [37], pyrene and coronene [38]) were produced in a similar fashion; therefore, the new 399 nm absorption system is assigned to $HCora^+$. The absorptions starting at 707 nm are of HCora.

Corannulene possesses three energetically non-equivalent protonation sites: *hub*, *rim*, and *spoke* (Chart 2SI). According to DTF/PBE0 and *ri*-MP2 calculations, the lowest energy $C_{20}H_{11}^+$ structure is the *hub*-isomer. The next in energy, *rim*, is located 7 and 20 kJ, mol^{-1} above *hub* by these methods. The relative energies of protonated corannulenes shown in Chart 2SI agree well with the ones calculated using the larger cc-pVTZ basis set [16].

Vertical excitation energies of the three isomers of $HCora^+$ were calculated with TDDFT, SAC-CI, and the second-order approximated coupled cluster (CC2) method implemented in Turbomole [34]. The equilibrium coordinates obtained from the to DTF/PBE0 and *ri*-MP2 calculations were used. The excitation energies and the oscillator strengths of *hub*- and *rim*-$HCora^+$ are given in Table 4 and for *spoke* in Table 5SI, because it is less likely produced in the source. It can be expected that both *hub* and *rim* structures of $C_{20}H_{11}^+$ should be present in the matrix, as was observed for other protonated PAHs [37, 38] when the ground state energies of isomers do not differ much.

All the methods predict two strong electronic transitions with $f > 0.1$ to the $1\,^1A'$ and $3\,^1A''$ excited electronic states of *hub* cation in the energy range below 4 eV. The $1\,^1A'$ state is predicted to be 1.8–2.7 eV above $X\,^1A'$ depending on the method used (Table 4). The calculations locate the $3\,^1A''$ state 3.6–4.0 eV above $X\,^1A'$. Computations at the same level of theory on *rim*-$C_{20}H_{11}^+$ also predict two strong electronic transitions in the energy range below 4 eV. The transition is predicted at the $3\,^1A$ excited state, lying in a similar energy range (1.9–2.6 eV) to the $1\,^1A'$ state of the *hub*-isomer. The next one is found at the $4\,^1A$ excited state located at 3.0–3.5 eV above the $X\,^1A$ one (Table 4).

The electronic spectrum measured following mass-selective deposition of $m/z = 251$ ions in a neon matrix is dominated by the strong absorption system (Figure 4) commencing at ≈ 399 nm (3.10 eV). A weak, broad, cationic feature is observed in a neon matrix at ≈ 515 nm, not shown in Figure 4. Corannulene cation substituted with a methyl, chloromethyl, di- and tri-chloromethyl groups were investigated in solutions with an absorption at ≈ 588 nm in C_6D_6 [15]. The wavelength of the absorption is far from the present observation for $HCora^+$, but quite close to the origin of $Cora^+$ in a neon matrix (601.2 nm). This suggests that the substitution of corannulene cation with a methyl or chloromethyl group slightly

Table 4: Excitation energies in eV and oscillator strengths of *hub*- and *rim*-isomers of $HCora^+$ calculated with TDDFT, SAC-CI, and CC2 methods using ground state equilibrium structures obtained from DFT/PBE0 and *ri*-MP2.

hub-$X\,^1A'$				
	TDDFT/PBE0	SAC-CI/PBE0	SAC-CI/MP2	CC2/MP2
$1\,^1A'$	2.67 0.09	1.80 0.1	1.77 0.1	2.53 0.1
$2\,^1A'$	3.74 0.03	3.34 0.05	3.22 0.04	3.61 0.06
$3\,^1A'$	3.89 0.02	3.52 0.01	3.56 0.005	3.90 0.005
$4\,^1A'$	4.22 0.2	3.94 0.3	3.80 0.3	4.13 0.3
$5\,^1A'$	4.45 0.03	4.28 0.004	4.21 0.004	4.27 0.004
$1\,^1A''$	2.32 0.004	1.75 0.03	1.77 0.06	2.35 0.02
$2\,^1A''$	2.66 0.05	1.82 0.04	1.79 0.0	2.54 0.05
$3\,^1A''$	3.96 0.2	3.82 0.2	3.57 0.2	3.88 0.2
$4\,^1A''$	4.66 0.0	4.47 0.04	4.61 0.05	4.57 0.02
$5\,^1A''$		4.80 0.04	5.00 0.5	4.78 0.05
rim-$X\,^1A$				
	TDDFT/PBE0	SAC-CI/PBE0	SAC-CI/MP2	CC2/MP2
$1\,^1A$	1.88 0.003	1.19 0.003	1.15 0.003	1.78 0.007
$2\,^1A$	2.14 0.007	1.54 0.01	1.46 0.01	2.11 0.01
$3\,^1A$	2.60 0.09	1.94 0.08	1.88 0.08	2.46 0.1
$4\,^1A$	3.47 0.1	3.03 0.2	3.01 0.2	3.37 0.2
$5\,^1A$	3.78 0.02	3.64 0.02	3.50 0.02	3.81 0.03
$6\,^1A$	4.00 0.06	3.95 0.09	3.83 0.1	4.09 0.06
$7\,^1A$	4.30 0.01	4.29 0.03	4.18 0.04	4.31 0.006
$8\,^1A$	4.32 0.02	4.36 0.05	4.24 0.05	4.35 0.02

perturbs the energy levels of $Cora^+$. A similar regularity was observed for diacetylene [39] and triacetylene cations [40] substituted with CH_3, where the origin of the first electronic transition is blue shifted by ≈ 16 and 2 nm, respectively, in comparison to unsubstituted cations. Addition of a hydrogen atom to polyacetylene cations greatly changes the electronic structure. The wavelength of the electronic transition, e.g. triacetylene cation is blue shifted by ≈ 226 nm under protonation [39]. A similar trend is also observed for $Cora^+$ and $HCora^+$ where the wavelengths of the origins differ by ≈ 200 nm.

Though the *hub*- and *rim*-structures of $HCora^+$ have similar ground state energies (Chart 2) only one isomer is observed in a neon matrix. The calculated excitation energies of *rim*-$HCora^+$ are in agreement with the origin at 399 nm; therefore, this band system is assigned to the $4\,^1A \leftarrow X\,^1A$ electronic transition of this cation. The strongest feature is the origin band, and a distinct vibrational structure is apparent in the spectrum (Figure 4). Due to the low symmetry, excitation of all 87 normal modes is allowed; therefore, no specific vibrational assignment

of the absorption bands has been made. One of the strongest features in the spectrum of HCora$^+$ above the origin is the 1450 cm^{-1} band. This is most probably due to a scissor-like vibration of the CH_2 group with a characteristic frequency of 1465 cm^{-1} [41].

Calculations (Table 4) predict another strong transition of *rim*-HCora$^+$ in the 1.9–2.6 eV energy range. At 515 nm (2.41 eV) a weak, broad, cationic feature is observed in a neon matrix (not shown in Figure 4). This absorption is assigned to the $3\,^1A \leftarrow X\,^1A$ electronic transition of *rim*-HCora$^+$.

Because the absorptions of *rim*-HCora$^+$ were detected in a neon matrix, the features which gain intensity after neutralization of the cations belong to neutral hydrogenated corannulene. These are: the 707.0 nm system and absorptions at 385.4, 343.6, 319.3, 303.7 nm (Table 5). To assign them to a specific electronic transition, SAC-CI and MS(8)-CASPT2 (11,12) calculations have been carried out. The excitation energies of HCora are given in Table 6. According to SAC-CI the first electronic transition is at 2.94 eV with $f = 0.004$, which can be compared with the 1.75 eV (707 nm) experimental value. An error of ≈ 1.20 eV is too large for these calculations to be used for an assignment of the HCora spectrum. The lowest energy transition, $1\,^2A \leftarrow X\,^2A$, calculated with CASPT2 is at 2.20 eV with $f = 0.01$, close to the observed absorption, and the adiabatic excitation energy should be ≈ 0.5 eV lower. The calculations predict several electronic transitions in the UV where absorptions of HCora were detected and assignments are given in Table 5.

3.2.2 Gas phase at 15 K

HCora$^+$, produced in reactions of protonated toluene with Cora within the source, was studied in the gas phase at 15 K by observing the $C_{20}H_{10}{}^+$ yield from photodissociation. The $3\,^1A$ excited state lies below the ≈ 2.5 eV thermodynamic threshold for H loss. Therefore, one photon promotes $C_{20}H_{11}{}^+$ to a level of the $3\,^1A$ state and the second into the fragmentation continuum. A weak electronic transition around 520 nm and a much stronger one commencing at 396.55 nm were detected (Table 5). The 520 nm feature is broad and no vibrational structure in the $3\,^1A \leftarrow X\,^1A$ electronic transition is discernible. The fwhm of this absorption points to a ≈ 5 fs lifetime in the $3\,^1A$ state.

The 397 nm system is compared with the spectrum of *rim*-HCora$^+$ measured in a 6 K neon matrix (Figure 5). The origin of the $4\,^1A \leftarrow X\,^1A$ electronic transition in the gas phase is blue shifted by ≈ 140 cm^{-1} with respect to the position in a neon matrix. The gas-phase to matrix shift is within the expected 1% energy range of the electronic transition [42]. Excess excitation energy of $4\,^1A$ was sufficient for photodissociation; however, two photons were absorbed so that $C_{20}H_{10}{}^+$

Table 5: Observed band maxima in the $3,4\,^1\mathrm{A} \leftarrow X\,^1\mathrm{A}$ electronic transitions of protonated corannulene in a 6 K neon matrix and the gas phase at 15 K. The absorptions in the $1,4,5,6\,^2\mathrm{A} \leftarrow X\,^2\mathrm{A}$ electronic transitions of hydrogenated corannulene in a 6 K neon matrix are also presented.

λ/nm	λ^{-1}/cm^{-1}	$\Delta\tilde{\nu}$/cm^{-1}	$\tilde{\nu}$/cm^{-1} [a]	$\Delta\tilde{\nu}$/cm^{-1} [a]	Assignment
HCora$^+$					
515.1	19 412	0	19 200	0	$3\,^1\mathrm{A} \leftarrow X\,^1\mathrm{A}$
398.8	25 075	0	25 219	0	$4\,^1\mathrm{A} \leftarrow X\,^1\mathrm{A}$
396.8	25 202	127	25 342	123	ν_{87}
			25 464	245	$2 \times \nu_{87}$
394.4	25 355	280	25 510	291	ν_{81}
392.3	25 491	416	25 628	409	ν_{77}
389.7	2 5661	586			
387.4	25 813	738			
384.0	26 042	967			
381.0	26 247	1172			
377.0	26 525	1450			
372.7	26 831	1756			586 + 1172
367.1	27 241	2166			416 + 1756
364.4	27 442	2367			2 × 1172
361.5	27 663	2588			1172 + 1450
359.0	27 855	2780			416 + 2 × 1172
357.0	28 011	2936			1172 + 1756
355.4	28 137	3062			
353.9	2 8257	3182			
HCora					
707.0	14 144	0			$1\,^2\mathrm{A} \leftarrow X\,^2\mathrm{A}$
688.3	14 529	385			
635.1	15 746	1602			
343.6	29 104	0			$4\,^2\mathrm{A} \leftarrow X\,^2\mathrm{A}$
319.1	31 338	0			$5\,^2\mathrm{A} \leftarrow X\,^2\mathrm{A}$
303.7	32 927	0			$6\,^2\mathrm{A} \leftarrow X\,^2\mathrm{A}$

[a] gas-phase values

was detectable on a microsecond timescale. The origin band of the $4\,^1\mathrm{A} \leftarrow X\,^1\mathrm{A}$ electronic transition of $C_{20}H_{11}{}^+$ was scanned with a dye laser; however, no rotational structure was apparent. The width of the origin band points to a ≈ 0.2 ps lifetime in the $4\,^1\mathrm{A}$ state.

Well-resolved vibrational structure is seen for the $4\,^1\mathrm{A} \leftarrow X\,^1\mathrm{A}$ electronic transition of $C_{20}H_{11}{}^+$ in the gas phase. The next most intense absorption lies 123 cm^{-1} to higher energy of the origin band. In the matrix spectrum, a weak shoulder 127 cm^{-1} to the blue of the origin is present. This band is assigned to

Table 6: Excitation energies in eV and oscillator strengths of *rim*-HCora calculated with SAC-CI and MS(8)-CASPT2 (11,12) using equilibrium coordinates obtained from DFT/PBE0.

CASPT2		SAC-CI	
$X\,^2$A		$X\,^2$A	
$1\,^2$A	2.20 0.01	$1\,^2$A	2.94 0.004
$2\,^2$A	2.53 0.004	$2\,^2$A	3.25 0.01
$3\,^2$A	2.75 0.003	$3\,^2$A	3.36 0.01
$4\,^2$A	2.93 0.06	$4\,^2$A	4.27 0.04
$5\,^2$A	3.15 0.03	$5\,^2$A	5.45 0.04
$6\,^2$A	4.12 0.007	$6\,^2$A	5.51 0.02
$7\,^2$A	4.28 0.002		

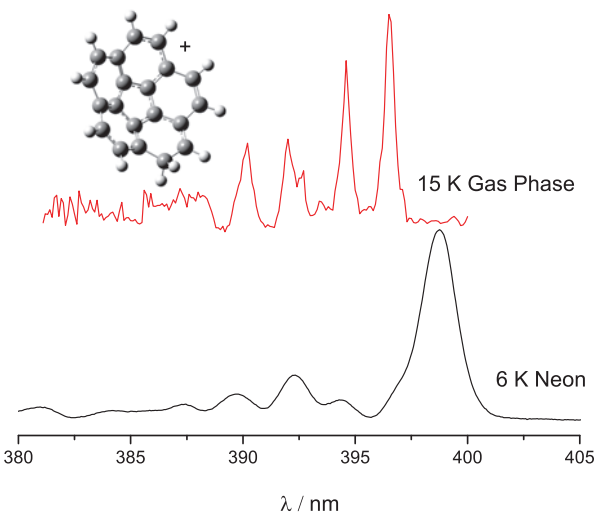

Figure 5: The $4\,^1$A ← $X\,^1$A electronic transition of protonated coranulene detected in a 6 K neon matrix (black trace) and the spectrum in the gas phase at 15 K (red trace).

the CH_2 rocking mode ν_{87} of the protonation site on the basis of the vibrational frequencies calculated with the DFT method (Table 1SI). The calculated energy of this mode is 127 cm^{-1}. This excited-state frequency of ν_{87} is more than double in protonated pyrene and coronene for a similar nuclear motion [43, 44]. This is due to the tertiary structure of $C_{20}H_{11}{}^+$. Double quanta excitation of ν_{87} in the $4\,^1$A state is also observed at 25 464 cm^{-1}. The ν_{87}, $2\nu_{87}$, ν_{81} and ν_{77} vibronic bands in the $4\,^1$A excited state have 50–90% of the intensity of the origin and are stronger than these observed in the neon matrix. This reflects a dependence of the dissociation rate on the excess excitation energy supplied to the cation. Photofragmen-

tation takes place from an highly excited vibration in the ground state of $HCora^+$ and leads to the formation of $Cora^+$ and H. This is similar for protonated pyrene and coronene [43, 44]. The band maxima of the $4\,^1A \leftarrow X\,^1A$ transition are given in Table 5.

4 Concluding remarks

Three structural forms of $C_{20}H_{10}{}^+$: cyclobutadieno-benzo[ghi]fluoranthene cation ($CBBF^+$) and two J-T distorted $Cora^+$ structures were detected in a 6 K neon matrix following deposition of $m/z = 250$ ions. $Cora^+$ was also produced via a charge-exchange reaction of Ar^+ with neutral corannulene and only the latter two structures were detected. The absorptions of $C_{20}H_{10}{}^+$ at 624.1, 601.2, and 590.0 nm were assigned to the $4\,^2A'' \leftarrow X\,^2A''$, $3\,^2A' \leftarrow X\,^2A''$, and $3\,^2A'' \leftarrow X\,^2A'$ electronic transitions of $CBBF^+$ and bowl-shaped $Cora^+$ structures, respectively, based on calculated excitation energies.

Protonated and hydrogenated Cora were studied in a 6 K neon matrix and the former also in the gas phase at 15 K in an ion trap via two-photon dissociation. Corannulene possesses three energetically non-equivalent protonation sites: *hub*, *rim*, and *spoke*. The former is the lowest energy isomer of $C_{20}H_{11}{}^+$ and a *rim*-structure lies slightly higher in energy. Excitation energies of *rim*-$C_{20}H_{11}{}^+$, calculated with TDDFT, SAC-CI, and CC2 methods, are in better agreement with the observed electronic spectrum than that of the *hub*-isomer. The strong, well-structured absorptions starting at around 399 nm are assigned to the $4\,^1A \leftarrow X\,^1A$ transition of *rim*-$HCora^+$. $HCora^+$ is the second largest PAH system after protonated coronene [38] for which an electronic absorption spectrum has been measured. In contrast to protonated pyrene and coronene, the strongest electronic transition of $HCora^+$ falls in the long-wavelength UV range, where DIBs have not yet been detected. Among the three H-PAHs$^+$, the 487 nm band system of $HPyr^+$ is the most intense. That of $HCor^+$ at 696 nm is two times less intense compared to $HPyr^+$, while that of $HCora^+$ at 399 nm is about ten times weaker. All transitions were normalized to the same deposited charge within the matrix.

Acknowledgement: This work was supported by the European Research Council (ERC-AdG-ElecSpecIons:246998) and the Swiss National Science Foundation (Project No. 200020-124349/1). The Siegel Group, especially A. Butterfield, is thanked for the sample preparation.

References

1. C. Jäger, F. Huisken, H. Mutschke, I. L. Jansa, and T. Henning, Astrophys. J. **696** (2009) 706.
2. A. Pathak and S. Rastogi, Astron. Astrophys. **485** (2008) 735.
3. P. Thaddeus, Philos. T. R. Soc. B **361** (2006) 1681.
4. http://www.astro.uni-koeln.de/cdms/molecules (cited March 12, 2015).
5. T. P. Snow and, V. M. Bierbaum, Annu. Rev. Anal. Chem. **1** (2008) 229.
6. A. Tielens, Annu. Rev. Astron. Astr. **46** (2008) 289.
7. F. J. Lovas, R. J. McMahon, J.-U. Grabow, M. Schnell, J. Mack, L. T. Scott, and R. L. Kuczkowski, J. Am. Chem. Soc. **127** (2005) 4345.
8. P. Pilleri, D. Herberth, T. F. Giesen, M. Gerin, C. Joblin, G. Mulas, G. Malloci, J.-U. Grabow, S. Brünken, L. Surin, B. D. Steinberg, K. R. Curtis, and L. T. Scott, Mon. Not. R. Astron. Soc. **397** (2009) 1053.
9. J. Cami, J. Bernard-Salas, E. Peeters, and S. E. Malek, Science **329** (2010) 1180.
10. O. Berné and A. G. G. M. Tielens, P. Natl. Acad. Sci. USA **109** (2012) 401.
11. L. T. Scott, H. E. Bronstein, D. V. Preda, R. B. M. Ansems, M. S. Bratcher, and S. Hagen, Pure Appl. Chem. **71** (1999) 209.
12. A. V. Zabula, S. N. Spisak, A. S. Filatov, A. Y. Rogachev, and M. A. Petrukhina, Angew. Chem. Int. Ed. **50** (2011) 2971.
13. S. N. Spisak, A. V. Zabula, A. S. Filatov, A. Y. Rogachev, and M. A. Petrukhina, Angew. Chem. **123** (2011) 8240.
14. M. Juríček, N. L. Strutt, J. C. Barnes, A. M. Butterfield, E. J. Dale, K. K. Baldridge, J. F. Stoddart, and J. S. Siegel, Nat. Chem. **6** (2014) 222.
15. C. Dubceac, A. V. Zabula, A. S. Filatov, F. Rossi, P. Zanello, and M. A. Petrukhina, J. Phys. Org. Chem. **25** (2012) 553.
16. A. Y. Rogachev, A. S. Filatov, A. V. Zabula, and M. A. Petrukhina, Phys. Chem. Chem. Phys. **14** (2012) 3554.
17. H. A. Galué, C. A. Rice, J. D. Steill, and J. Oomens, J. Chem. Phys. **134** (2011) 054310.
18. J. Seiders, E. L. Elliott, G. H. Grube, and J. S. Siegel, J. Am. Chem. Soc. **121** (1999) 7804.
19. P. Freivogel, J. Fulara, D. Lessen, D. Forney, and J. P. Maier, Chem. Phys. **189** (1994) 335.
20. E. P. L. Hunter and S. G. Lias, J. Phys. Chem. Ref. Data **27** (1998) 413.
21. F.-X. Hardy, C. A. Rice, O. Gause, and J. P. Maier, J. Phys. Chem. A **119** (2014) 1568.
22. D. Gerlich, Adv. Chem. Phys. **82** (1992) 1.
23. J. P. Perdew, K. Burke, and M. Ernzerhof, Phys. Rev. Lett. **77** (1996) 3865.
24. J. P. Perdew, K. Burke, and M. Ernzerhof, Phys. Rev. Lett. **78** (1997) 1396.
25. J. Dunning and T. H., J. Chem. Phys. **90** (1989) 1007.
26. A. D. Becke, J. Chem. Phys. **98** (1993) 5648.
27. C. Lee, W. Yang, and R. G. Parr, Phys. Rev. B **37** (1988) 785.
28. G. Rouillé, C. Jäger, M. Steglich, F. Huisken, T. Henning, G. Theumer, I. Bauer, and H.-J. Knölker, ChemPhysChem **9** (2008) 2085.
29. M. J. Frisch, G. W. Trucks, H. B. Schlegel, G. E. Scuseria, M. A. Robb, J. R. Cheeseman, G. Scalmani, V. Barone, B. Mennucci, G. A. Petersson, H. Nakatsuji, M. Caricato, X. Li, H. P. Hratchian, A. F. Izmaylov, J. Bloino, G. Zheng, J. L. Sonnenberg, M. Hada, M. Ehara, K. Toyota, R. Fukuda, J. Hasegawa, M. Ishida, T. Nakajima, Y. Honda, O. Kitao, H. Nakai, T. Vreven, J. A. Montgomery Jr., J. E. Peralta, F. Ogliaro, M. Bearpark, J. J. Heyd, E. Brothers, K. N. Kudin, V. N. Staroverov, R. Kobayashi, J. Normand, K. Raghavachari, A. Rendell,

J. C. Burant, S. S. Iyengar, J. Tomasi, M. Cossi, N. Rega, J. M. Millam, M. Klene, J. E. Knox, J. B. Cross, V. Bakken, C. Adamo, J. Jaramillo, R. Gomperts, R. E. Stratmann, O. Yazyev, A. J. Austin, R. Cammi, C. Pomelli, J. W. Ochterski, R. L. Martin, K. Morokuma, V. G. Zakrzewski, G. A. Voth, P. Salvador, J. J. Dannenberg, S. Dapprich, A. D. Daniels, Ö. Farkas, J. B. Foresman, J. V. Ortiz, J. Cioslowski, and D. J. Fox, Gaussian 09 Revision D.01, Gaussian Inc., Wallingford CT (2009).

30. H. Nakatsuji and K. Hirao, J. Chem. Phys. **68** (1978) 2053.
31. H. Nakatsuji, Chem. Phys. Lett. **67** (1979) 329.
32. J. Finley, P. Malmqvist, B. O. Roos, and L. Serrano-Andrés, Chem. Phys. Lett. **288** (1998) 299.
33. F. Aquilante, L. De Vico, N. Ferré, G. Ghigo, P. Malmqvist, P. Neogrády, T. B. Pederson, M. Pitoňák, M. Reiher, B. O. Roos, L. Serrano-Andrés, M. Urban, V. Veryazov and R. Lindh, J. Comput. Chem. **31** (2010) 224.
34. R. Ahlrichs, M. Bar, M. Haser, H. Horn, and C. Kolmel, Chem. Phys. Lett. **162** (1989) 165.
35. T. Sato, A. Yamamoto, and H. Tanaka, Chem. Phys. Lett. **326** (2000) 573.
36. I. Garkusha, A. Nagy, J. Fulara, M. F. Rode, A. L. Sobolewski, and J. P. Maier, J. Phys. Chem. A **117** (2013) 351.
37. I. Garkusha, J. Fulara, A. Nagy, and J. P. Maier, Astrophys. J. **728** (2011) 131.
38. I. Garkusha, J. Fulara, P. J. Sarre, and J. P. Maier, J. Phys. Chem. A **115** (2011) 10972.
39. J. P. Maier, O. Marthaler, and E. Kloster-Jensen, J. Chem. Phys. **72** (1980) 701.
40. A. Chakraborty, J. Fulara, and J. P. Maier, Aust. J. Chem. **67** (2013) 416.
41. D. Lin-Vien, N. B. Colthup, W. G. Fateley, and J. G. Grasselli, *The Handbook of Infrared and Raman Characteristic Frequencies of Organic Molecules*, Elsevier, San Diego (1991).
42. M. E. Jacox, J. Phys. Chem. Ref. Data **27** (1998) 115.
43. F.-X. Hardy, O. Gause, C. A. Rice, and J. P. Maier, Astrophys. J. Lett. **778** (2013) L30.
44. C. A. Rice, F.-X. Hardy, O. Gause, and J. P. Maier, J. Phys. Chem. Lett. **5** (2014) 942.

Supplementary material: The online version of this article
(DOI: 10.1515/zpch-2015-0598) provides supplementary material for authorized users.